The Determination of Brønsted Acid Sites in Zeolite ERS-7 by Neutron and X-ray Powder Diffraction

B. J. Campbell* and A. K. Cheetham

Materials Research Laboratory, University of California, Santa Barbara, California 93106

T. Vogt

Physics Department, Brookhaven National Laboratory, Upton, New York 11973

L. Carluccio, W. O. Parker, Jr., C. Flego, and R. Millini

EniTecnologie S.p.A., Via F. Maritano 26, I-20097 San Donato Milanese, MI-Italy

Received: August 1, 2000; In Final Form: November 20, 2000

The deuterated acid form of zeolite ERS-7 (Si/Al = 8.4) has been prepared by repeated cycles of D_2O exposure and calcination. ^{27}Al NMR data show that the relative proportions of tetrahedral and octahedral Al in the resulting material are 70 and 30%, respectively. Three Brønsted sites were identified by a combined Rietveld refinement that simultaneously employed synchrotron X-ray powder diffraction data and neutron powder diffraction data. Final lattice parameters were $a = 9.7843(1)$ Å, $b = 12.3676(1)$ Å, and $c = 22.8336(2)$ Å, the combined R_{wp} factor was 6.3%, and χ^2(reduced) was 1.48. Acid deuterons were located approximately 1 Å from oxygens O3, O5, and O7, with occupancy factors of 0.16(2), 0.16(3), and 0.18(2), respectively. These correpsond to 1.28(16), 0.64(12), and 1.44(16) deuterons per unit cell, respectively, for a total of 3.36(26) acid sites per unit cell, which is consistent with the tetrahedral Al content. Only deuteron D5 lies on a special position. T−O bond lengths suggest a site preference for Al at T4, T1, and possibly T2, each of which is bonded to at least one of the observed acid-site oxygens. A bridging framework oxygen site was identified in both the PND and PXD difference Fourier maps that appears to be disordered over at least two distinct sites; this corresponds to different local arrangements of Al at the neighboring T-sites. The out-of-plane framework hydroxyl tilt angles at each acid site were comparable to those of H^+ SSZ-13 and D^+ RHO. Acid site D7 demonstrated a significant in-plane hydroxyl tilt angle (7.5°), consistent with ab initio quantum mechanical calculations. This tilt clearly indicates an Al preference for site T4 over T6.

Introduction

Acidic zeolite catalysts are widely used in the chemical and petroleum industries for their catalytic activity, their remarkable reaction selectivity, and their excellent chemical and thermal stability.[1] Important applications include the isomerization of xylenes, paraffin hydroisomerization, catalytic cracking, and heavy oil hydrocracking.[2,3,4] The principal mechanism of acidity in these materials is the donation of Brønsted acid protons from bridging framework hydroxyls. Acid protons balance the negative charge that is acquired by the otherwise neutral framework when Al^{3+} ions occupy some of the tetrahedrally coordinated Si^{4+} sites. Both natural and synthetic aluminosilicate zeolites can be converted to the acid form from other cationated forms by ion exchange with an NH_4 salt and subsequent calcination to remove NH_3.

A Brønsted acid proton interacts with the framework in a very different way than do other cations; rather than ionically coordinating to multiple framework oxygens, it covalently bonds to one of the oxygens adjacent to a tetrahedral Al atom and significantly distorts the local framework bonds and angles.[5] Recent computational studies have shown that the geometry of the framework in the vicinity of an acid site can significantly influence the formation of the intermediate species that lead to the final reaction products.[6,7] Ab initio cluster calculations of ethylene adsorption on a high-silica acid zeolite, for example, suggest the formation of an intermediate ethoxide that forms a C−O bond to a nearby framework oxygen.[8,9] Because the local structure of an acid site controls acidity, accessibility by reactant molecules, intermediate state formation, and hence the reaction product, the knowledge of its locations and environments within the framework is critical to better understanding acid zeolite catalysis.

Several diffraction-based approaches have been used to determine the locations of Brønsted acid sites in zeolites and other silicates. Early inferences were based on average Si−O bond lengths, as determined by X-ray diffraction,[10] which are expected to increase upon protonation in proportion to the acid site occupancy factor. In $Ca_3(SiO_3OH)_2(H_2O)_2$ (afwillite) and $Na_2H_2(SiO_4)(H_2O)_8$, for example, certain Si−O bonds were observed to be 0.08 Å longer than the others, on average, and were attributed to the formation of an acidic hydroxyl.[11,12] Based on these observations, Olson and Dempsey investigated T−O (T = Si, Al) distances in acidic zeolite Y (Si/Al = 2.3) via single crystal X-ray diffraction, compared them to those of other acidic faujasite zeolites, and concluded that the O1 and O3 sites were preferentially protonated while the other framework oxygens were not.[13]

* Corresponding author. Present address: Argonne National Laboratory, Materials Science Division, Argonne, IL 60439. E-mail: branton@anl.gov.

10.1021/jp002751t CCC: $20.00
Published on Web 02/15/2001

Preferred acid sites correlate to the preferred framework Al sites that they compensate. While it is difficult to distinguish between Si and Al using standard X-ray diffraction techniques, due to their similar scattering cross sections, Al occupancy can be inferred from average T−O distances.[14] The average T−O distance around a T-site that is preferentially occupied by Al will have an intermediate value between the ideal Si−O (1.61 Å) and Al−O (1.74 Å) distances.[15,16] This approach has been exploited for predicting T-site-specific Al occupancies in a variety of zeolites.[14,17] Mortier et al.[18] made use of inferred Al occupancies in an attempt to predict acid-site locations in a single crystal of acidic zeolite mordenite, but were unable to conclusively identify any preferred sites within experimental and statistical uncertainties. Alberti also investigated acidic mordenite, drawing upon several published structures and making estimates of their T-site Al occupancies.[19] He then deduced a proton distribution that was compatible with these occupancies and concluded that acid protons occupy sites within both the main 12-membered-ring (12MR) channels and the twisted 8MR channels, in agreement with previous IR investigations.[20]

Computational techniques have also provided important insight into the problem of acid proton siting and acid-site geometry in zeolites. Studies of absolute acid strength, for example, have implications for acid proton siting, because those protons that are most tightly bound to the framework are also the most energetically favorable and, therefore, the most likely to be populated. Eichler et al.[21] examined all four potential acid sites in zeolite Y, using the QM-Pot embedded cluster approach, and determined O1 to be the most favorable site followed by O3; this is in agreement with other experiments. Brandle and Sauer[6] calculated the primary acid proton locations in the zeolites faujasite (FAU), chabazite (CHA), mordenite (MOR), and ZSM-5 (MFI) using a similar approach and compared their stabilities on an absolute scale. Computational studies have been particularly helpful in unraveling the effect of Al siting on the binding energies of acid protons;[22−24] the energies tend to increase with the number of next-nearest-neighbor aluminums.

Neutron diffraction is the most direct experimental method used to probe Brønsted acid siting because neutrons interact strongly enough with hydrogen nuclei to have a significant effect on Bragg peak intensities. ^{2}H (deuterium) is the most desirable isotope for use in neutron diffraction experiments because it has both an unusually large coherent scattering cross section and a tolerably small incoherent scattering cross section. The first neutron powder diffraction (PND) refinement of acid deuteron occupancies and positions in a zeolite was published by Jirak et al.;[25] it made use of four samples of partially acidic mixed-cation zeolite, Y, which possessed different acid-site concentrations. Acid-site locations were estimated from the framework geometry (1 Å from each oxygen along the bisector of the obtuse T−O−T angle), inserted into the model, and their occupancies refined; this led to the conclusion that the O1 and O3 sites were preferentially protonated while the O2 and O4 sites were not, in agreement with the observations of Olson and Dempsey.[13] Similar conclusions were reached by Czjzek et al.[26] who performed a full refinement of the framework and acid-site positions and occupancies of zeolite Y and reported evidence of Brønsted acid sites in the Fourier difference maps of both the protonated and deuterated samples. Cheetham et al.[27] performed a PND study of zeolite Y in the hydrated La form, and observed not only a Brønsted acid site, but also the hydrolyzed cation that was responsible for its formation.

Two detailed investigations of the deuterated acid form of zeolite RHO (Si/Al = 7)[28,29] reported a single bridging hydroxyl bonded to its framework O1 oxygen site; this site had the smallest T−O−T angle in the framework. Because the deuterons were difficult to locate by difference Fourier analysis, a grid search was performed in which the position of a dummy atom was varied and its occupancy was refined. The authors reported that candidate positions obtained using this technique can usually be refined successfully. Though the deuteron concentration was low, the T−O1 distance in each sample was significantly larger than the T−O2 distance, which indicated preferential O1 protonation. Two distinct proton acid sites were identified by Smith et al.[30] in an acidic high-silica CHA analogue known as SSZ-13; the same two sites were also observed in the deuterated acidic silico-alumino-phosphate CHA analogue, SAPO-34.[31]

Zeolites FAU, RHO, and CHA each have relatively simple structures, making them ideal materials for the investigation of subtle features such as Brønsted acid sites. However, PND studies of Brønsted acid sites were recently reported by Martucci and co-workers for zeolites ferrierite (FER)[32] and MOR,[33] which are considerably more complex. D^+ FER exhibits a surprising acid site preference at two of its eight independent oxygen sites, though the occupancies at these sites were sufficiently low (15%) that increases in the corresponding T−O distances were unobservable. The acid sites in D^+ MOR were less tightly distributed; evidence was found for preferential siting at 4 of the 10 independent oxygen sites, while approximately half of the deuterons could not be located.

The recently discovered zeolite, ERS-7 (IZA code ESV), provides an ideal opportunity to study Brønsted acid sites in a new zeolite with potential catalytic applications. The determination of its framework structure by simulated annealing techniques and its structure refinement against high-resolution synchrotron powder diffraction data were recently reported by Campbell et al.[34] ERS-7 shows exceptional resistance to thermal and chemical degradation, and it maintains good crystallinity during the high-temperature calcinations required to prepare its acid form.[35,36] Though the ERS-7 framework is unusually complex (6 unique T-sites, 14 unique oxygens, and 56 independent positional parameters), the high information content of its X-ray powder diffraction pattern makes it suitable for the examination of subtle structural details.

Experimental Section

The preparation of a D^+ ERS-7 sample for X-ray and neutron diffraction experiments began with a sample of composition $DMP_{3.6}Na_{1.77}[Al_{5.16}Si_{42.84}O_{96}]\cdot nH_2O$ (DMP = *N*,*N*-dimethylpiperidinium), which was synthesized according to the original method.[35,36] This material was then converted to the H^+ form by calcination under flowing air at 873 K for 5 h, three overnight exchanges with ammonium acetate at 333 K, and another calcination at 873 K. The resulting material had an Si/Al ratio of 8.4 and appeared to be fully ion exchanged, with a residual Na/Al ratio of only 0.014.

The H/D exchange was first attempted using rehydrated H^+ ERS-7 in a concentrated ND_4OD/D_2O solution at an elevated temperature. After three cycles of ND_4 exchange, centrifugation, rinsing (with D_2O), and drying in an H_2O-free nitrogen atmosphere, the solid was dehydrated at 773 K and checked for residual protons by ^{1}H NMR, which revealed only a modest degree of proton to deuteron exchange (ca. 40%). Similar difficulties have been reported previously, and may be due to the slow exchange of the nonacidic silanols, which can then exchange protons with the deuterated bridging hydroxyls during

subsequent calcination and storage. Freude et al.,[37] for example, obtained a mere 75% H^+ to D^+ exchange after equilibrating H^+ Y with D_2O at 298 K for 7 days.

A greatly improved degree of exchange was obtained using vacuum line techniques. Several grams of H^+ ERS-7 were placed in a 10 mm quartz tube (25 mL), attached to a glass manifold vacuum line by a Rotoflo valve, and thoroughly dried for 10 h at 773 K and 10^{-3} Torr. This material was then loaded (2 mmol per gram of sample) with gaseous D_2O (99.5% D, Merck) in 10 sequential "cold-finger" transfers. In each transfer, the portion of the quartz tube containing the sample was immersed in liquid nitrogen and a measured volume of warm D_2O was released into this otherwise sealed and evacuated portion of the vacuum line. When the D_2O liquid was fully evaporated and readsorbed onto the sample, the loaded sample was left to equilibrate at room temperature for 5−10 days. It was then dried, loaded with D_2O, and equilibrated in the same way three more times. The degree of exchange obtained with this approach was 85% after two exchange cycles and 95% after four exchange cycles. A 2.5 g sample of the final D^+ ERS-7 product was then dehydrated again, at 773 K, and flame-sealed under 10^{-3} Torr vacuum in a quartz ampule for transport. Upon opening of the ampule in an argon-atmosphere glovebox (O_2 and H_2O < 1 ppm), the sample was immediately poured into a vanadium cannister which was then sealed with indium wire. A small amount of the sample was also tapped into a 1 mm quartz capillary, placed under a slight negative pressure, removed from the glovebox, and flame-sealed.

Quantitative ^1H NMR spectra were collected at 300.15 MHz, with ca. 90 mg of dry powder, in a 4 mm zirconia rotor that was spinning at 14 kHz on a Bruker CXP-300 spectrometer. Measurement parameters included 1 μs (25°) rf pulses, a 64 kHz spectral window, a 25 ms acquisition time, a 20 s recycle delay, and 500 scans. After the background signal that was obtained with an empty rotor was subtracted out, the integrated peak areas from the pre- and postexchanged samples were compared, including the spinning sidebands. Samples were loaded into predried zirconia rotors inside a nitrogen atmosphere glovebox.

PND data were collected at the high-resolution powder diffraction beamline[38] of the Australian Nuclear Science & Technology Organization's research reactor at Lucas Heights. Two data sets were collected, one at room temperature and one at 10 K, using a wavelength of 1.8857 Å. The sample was rotated around the axis of the cannister (vertical) during the room-temperature run, and then attached to a cryostat for the 10 K measurements. The detector, which consisted of 12 ^3He counters, was stepped in 0.05° intervals, such that the total 2θ range covered was 0−153°. The average counting time per point was about 5 min. Synchrotron X-ray powder diffraction (PXD) data were collected at beamline X7A of the national synchrotron light source at the Brookhaven National Laboratory. The monochromatic 1.1387 Å radiation was selected with a Ge[111] double-crystal monochromator, and the diffracted intensity was measured using a Ge220 analyzer and a standard scintillation detector over the range $3° \le 2\theta \le 63.5°$ in steps of 0.005°. The detection time began at 10 s per step and was doubled every 10° in 2θ. The horizontal incident and receiving slits were measured to be 12 and 16 mm, respectively, and the sample−detector distance was 700 mm. The sample was also rotated at ca. 1 Hz during data collection in order to minimize potential systematic errors which result from preferred orientation effects.

Results and Discussion

The unusual structural complexity of the ERS-7 framework made it necessary to employ both synchrotron X-ray powder diffraction (PXD) and PND in a simultaneous Rietveld refinement with both datasets. The high-resolution synchrotron data made it possible to refine the many degrees of freedom of the framework, while the neutron data served as the primary source of information about the acid sites. The advantage of simultaneously using both X-ray and neutron data is not only an increased number of observations, but also the ability to simultaneously probe structural features that lend themselves to one technique but not the other. One then incorporates the multiple complementary views of the same structure. While the use of simultaneous multi-dataset structure refinements is well established,[39] this approach does not appear to have been used for the determination of Brønsted acid sites. Previous applications of this technique include the structural analysis of the superconducting phases $YBa_2Cu_3O_{7-x}$[40] and $Bi_2Sr_2CaCu_2O_{8+x}$,[41] as well as $K(Ti_{0.5}Sn_{0.5})OPO_4$, which is a nonlinear optical material.[42]

PND/PXD Le Bail Profile Refinement. Before structure refinement was begun, the background, lattice parameters, profile shape, etc. were refined with a simultaneous Le Bail fit to both the PXD and PND patterns, using the multi-dataset capabilities of the GSAS[43] software suite. This produced the agreement indices $R_{wp(X)} = 5.1\%$, $R_{p(X)} = 4.9\%$, $DW_{d(X)} = 1.25$, $R_{wp(N)} = 3.5\%$, $R_{p(N)} = 2.9\%$, $DW_{d(N)} = 2.05$, $R_{wp(C)} = 4.7\%$, $R_{p(C)} = 4.6\%$, $DW_{d(C)} = 1.39$, and $\chi^2 = 0.8105$ (X for X-ray, N for neutron, C for combined, *R* for *R*-factor, and DW for Durbin−Watson[44] statistic). The refined parameters included a 20-term linear-interpolation background that was superimposed on a manually fitted fixed PXD background, a 15-term cosine-series background superimposed on a manually fitted fixed PND background, three lattice parameters, a zero error for each pattern, the Finger−Cox−Jephcoat asymmetry function[45] for the PXD profile, the isotropic Gaussian peak widths $GW_{PXD} = (0.08°)^2$ and $GW_{PND} = (1.66°)^2$, and the anisotropic broadening function described by Stephens[46] for the PXD profile: $S_{400} = 2.1$, $S_{040} = 2.8$, $S_{004} = 0.15$, $S_{220} = 1.0$, $S_{202} = 0.27$, and $S_{022} = 0.50$ (10^{-6} Å^{-4}). The low value of χ^2 (<1) is likely to be due to the way that the background was handled.

Framework Structure Refinement. Before the multi-dataset refinement was attempted, separate Rietveld refinements of the ERS-7 framework structure were first carried out using the PND data only and the PXD data only. Convergence was generally much easier to obtain with the PXD-only data, and the distribution of bond lengths and thermal parameters was twice as narrow: min(PND) = 1.514 Å, max(PND) = 1.731 Å, ave(PND) = 1.612 Å, esd(PND) = 0.063 Å; min(PXD) = 1.526 Å, max(PXD) = 1.708 Å, ave(PXD) = 1.601 Å, and esd(PXD) = 0.038 Å. Furthermore, the simultaneous use of both data sets in a combined refinement of the framework structure yielded an overall bond-length distribution almost identical to the results of the PXD-only refinement. Readers can compare the PXD-only bond-length distribution to the results obtained using the H^+ ERS-7 framework structure recently published by Campbell et al.:[34] min = 1.556 Å, max = 1.626 Å, average = 1.597 Å, and esd = 0.019 Å. The average value of F^2/σ is 15% lower for the D^+ PXD data than that obtained for the earlier H^+ data, and the average peak width has increased by 25%, despite the fact that the two data sets were collected with nearly identical instrumental settings.

These difficulties appear to be the consequences of a decrease in sample crystallinity resulting from the four additional high-

temperature treatments that are necessary to prepare the D^+ exchanged form. The practical result of the diminished information content of the PXD data was the need to impose some bond-length restraints on the framework T−O distances that grew extremely short (<1.56 Å) relative to the expected value of 1.6 Å. It is well known that such distances do not accurately reflect the local crystal chemistry. Instead, they either result from underdetermination, or else represent an average over some form of framework disorder. After convergence was achieved, all restraints were released and only those few T−O distances that persisted in dropping to low values were again restrained. Bond lengths that tended to values greater than the average were not interfered with so that information regarding aluminum siting, albeit limited, might be cautiously interpreted. Only a few select T−O distances grew noticeably large, possibly indicating a preference for Al on the T1 and T4 sites. The few bond-length restraints that were required do limit our ability to interpret the framework structure, but they also make it possible to begin the acid site search from a reasonable starting point.

Brønsted Acid Site Determination. The complexity of the ERS-7 framework and the subtlety of the features being investigated here made 3D viewing capabilities indispensable. Fourier difference maps were generated using GSAS and were superimposed, as constant density surfaces, on a 3D image of the framework. This was accomplished with the MSI Cerius[2] software suite,[47] which contains an interface to GSAS, and also with the new GSAS facility for producing 3D Fourier surfaces in VRML format, which can then be viewed and manipulated with any external VRML viewer. Both X-ray and neutron Fourier difference maps were generated using the framework model from the combined refinement. These difference maps were then superimposed in different colors. Peaks that occurred at the same location in both the X-ray and neutron difference maps were considered to be good candidate oxygen positions, whereas large peaks that appeared only in the neutron map were examined as potential acid sites.

The largest peak in the difference Fourier map (Figure 1) appeared to be a Brønsted acid site, located approximately 1 Å from O5 in the T−O−T plane. A deuteron, labeled D5, was inserted at this site and its occupancy was refined to about 20%, which is less than 1 deuteron per cell and only a fraction of the 5.1 deuterons that were expected on the basis of the Al content of the sample (Si/Al = 8.4). A visual search of the Fourier map turned up another likely candidate associated with O3 which also resulted in an occupancy of nearly 20%. The occupancy of D3 refined to 1.6 deuterons per cell for a total of 2.4 per cell. Because O3 is one of the oxygens of the eight-ring windows that make up the main channel system, D3 reaches out into the channel. D5, on the other hand, lies within one of the six-ring windows along the walls of the 17-sided ($4^6 5^4 6^5 8^2$) cage (see Figure 2).

Viewing the 3D Fourier maps was a fairly direct way of searching for potential Brønsted acid sites, and with this method we succeeded in identifying two of them. When this route had been exhausted, hypothetical acid-site locations were calculated for each of the 14 bridging framework oxygens; zero occupancy deuterons were inserted at each of these 14 positions, and all 14 occupancies were damped and refined simultaneously. Each hypothetical acid site was assumed to be 1 Å from the corresponding oxygen along the line bisecting the T−O−T angle, on the open side of the angle. Deuteron positions were then also damped and refined with stiff 1 Å D−O distance restraints. Sites that refined to negative or near-zero occupancies were eliminated, but several sites remained. Next, the framework

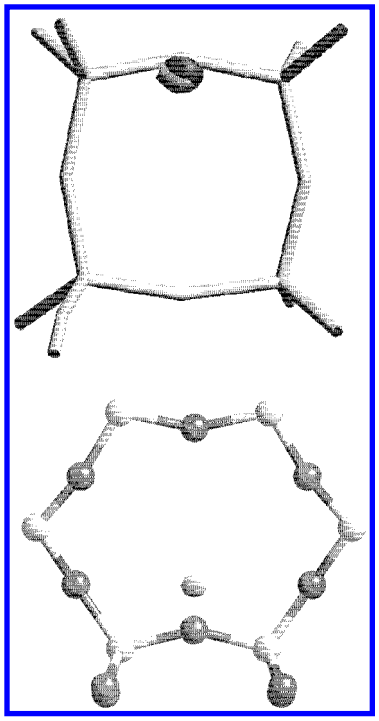

Figure 1. 3D difference Fourier surfaces from the combined X-ray/neutron Rietveld refinement of D^+ ERS-7. The peaks shown are the largest in the difference maps after refining only the framework atoms. Top: Both the neutron (light) and X-ray (dark) difference Fourier surfaces superimposed on the four-ring containing O11. This peak is evidence of an alternative oxygen position. Bottom: Neutron difference Fourier surface reveals a peak 1 Å from O5 along the bisector of the T−O−T angle. This peak is evidence of a Brønsted acid site.

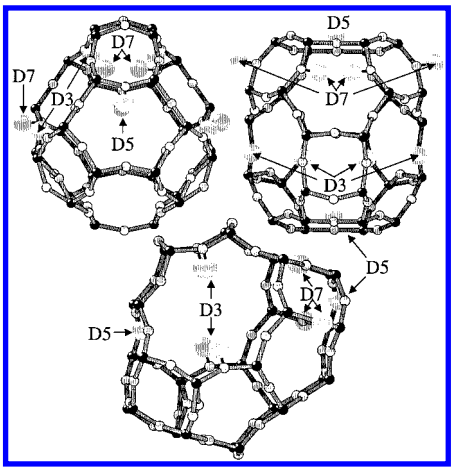

Figure 2. Locations of Brønsted acid site in D^+ ERS-7, obtained from a simultaneous refinement against both X-ray and neutron powder diffraction data. The main cage is viewed from three different direct ions.

was included in the refinement and the damping level was reduced. After a number of least-squares cycles, deuterons that persisted in oscillating wildly or drifting away from reasonable acid-site locations were eliminated from the model. Each of the eliminated deuteron sites was then reinserted one at a time for individual examination, but most were again discarded. The hypothetical site near O1 was given special attention due to the rather long T1−O1 bonds that suggested a significant Al population on T1, but the deuteron position persisted in drifting nearly 90° out of the T1−O1−T1 plane and was finally omitted. The only new acid site discovered via this method was labeled D7, because it refined consistently and robustly to a reasonable position 1 Å from O7. This deuteron also lies in a six-ring along

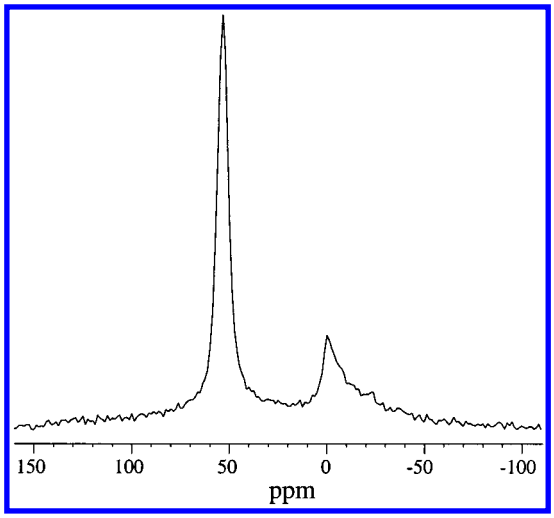

Figure 3. ^{27}Al MAS NMR spectrum from rehydrated D^+ ERS-7.

the side of the 17-sided cage, but it does not sit in the vicinity of a special crystallographic position. D3 and D5 were relatively insensitive to this process, and they converged nicely in each trial refinement.

So in addition to D3 and D5, which were found directly in the difference Fourier map, one new site, D7 (see Figure 2), was located by examining geometrically likely deuteron sites. Because all three of these acid sites do not bond to the same T-site, there must be more than one T-site that hosts framework Al. The ^{27}Al MAS NMR spectrum in Figure 3 reveals little about Al siting, since only a single featureless tetrahedral Al peak was observed at 54 ppm; a single peak could be the result of narrowly distributed isotropic shifts or insufficiently averaged quadrupolar interactions. The ^{27}Al NMR does, however, show that a significant amount (30%) of the Al in the sample has been removed from the tetrahedral framework sites during the high-temperature heat treatments that were required to prepare the D^+ exchanged form, and these were converted to octahedral Al (the 0 ppm peak). This is also consistent with the broader peaks and diminished $\langle F^2/\sigma \rangle$ values seen in the D^+ ERS-7 PXD data. The positional and occupancy parameters of each of the three deuteron acid sites refined to reasonable values, though it was necessary to impose slight damping (actual shift = 70% of calc. shift) and very loose D−O distance restraints (σ = 0.5 Å) on the deuterons in order to avoid small oscillations in the positional parameters. The deuteron isotropic thermal factors were fixed at U_{iso} = 0.025 Å^2 due to correlations with the occupancies. The refined occupancies add up to a total of 3.36-(26) deuterons per unit cell. This is less than the 5.1 deuterons per unit cell that were expected on the basis of the Si/Al ratio alone, but is consistent with the 3.6 deuterons per unit cell that was calculated by taking the octahedral Al into account. The parameters of the final model are found in Table 1.

The largest peak in the X-ray difference Fourier map coincided with the second-largest peak in the neutron difference map, at a position 1 Å from O11, but this is nearly 90° from the T−O−T plane, thus making it an unlikely candidate for an acid site. A deuteron was inserted into the model at this location and its occupancy was refined; this eliminated the corresponding peak in the neutron difference map, but hardly reduced the same peak in the X-ray difference map. Because the location of this Fourier difference peak, relative to O11 and to the adjacent T4 and T6 atoms, gave it the appearance of an alternate oxygen position (suggesting some framework disorder), the peak was instead replaced with an oxygen labeled as O11b, and O11 was relabeled as O11a. The occupancy factors of O11a and O11b were then refined freely to respective values of 65 and 45%. After the O11b position was freed, the sum of the two occupancies was fixed to 1.0, and T−O distance restraints were applied and then subsequently relaxed, the following parameters emerged: $Occ_a \approx 58\%$, $Occ_b \approx 42\%$, T4−O11a = 1.69 Å, T4−O11b = 1.59 Å, T6−O11a = 1.60 Å, and T6−O11b = 1.66 Å.

The T−O-T angles at O11a and O11b fold in almost opposite directions after refinement, and each angle possesses one long T−O bond and one short T−O bond. The T−O bond lengths of O11a and O11b are similar, though O11a has its long bond with T6 while O11b has its long bond with T4. The result is shown in Figure 4. Without restraints, the long bonds are approximately 1.7 Å and the short bonds are closer to 1.55 Å. These short bonds were among those restrained so as to keep them closer to the reasonable value of 1.6 Å, even though this also affected the lengths of the long bonds. Both sites were investigated for acid protons as a possible explanation of the long bonds, but none were observable there. The random partial

TABLE 1: Final Structural Parameters for D^+ ERS-7

atom	x	y	z	U_{iso} (Å^2)	occ
T1[a]	0.3388(3)	0.8734(3)	0.8639(1)	0.011(1)	0.895/0.105
T2	0.6449(3)	0.8744(3)	0.5304(2)	0.005(1)	0.895/0.105
T3	0.8864(3)	0.5163(3)	0.9182(1)	0.004(1)	0.895/0.105
T4	0.1535(3)	0.8740(3)	0.6537(1)	0.005(1)	0.895/0.105
T5	0.9635(3)	0.1227(3)	0.8091(2)	0.000(1)	0.895/0.105
T6	0.2272(3)	0.4833(3)	0.7604(2)	0.002(1)	0.895/0.105
O1	0.3029(8)	0.75	0.8401(5)	0.029(4)	1
O2	0.2686(7)	0.8973(5)	0.9248(3)	0.025(3)	1
O3	0.5020(6)	0.8894(5)	0.8702(3)	0.031(2)	1
O4	0.2853(8)	0.9512(6)	0.8133(4)	0.066(3)	1
O5	0.6381(10)	0.75	0.5135(5)	0.035(4)	1
O6	0.6657(6)	0.9489(5)	0.4728(3)	0.021(3)	1
O7	0.5037(8)	0.9016(5)	0.5610(3)	0.026(2)	1
O8	0.9441(6)	0.4389(5)	0.8697(2)	0.035(3)	1
O9	0.7625(6)	0.5852(5)	0.8930(3)	0.031(3)	1
O10	0.1809(10)	0.75	0.6736(5)	0.048(4)	1
O11a	0.1927(12)	0.5889(8)	0.7231(6)	0.012(3)	0.58(2)
O11b	0.3503(18)	0.0333(17)	0.2017(8)	0.012(3)	0.42(2)
O12	0.9595(9)	0.25	0.8231(4)	0.022(4)	1
O13	0.3456(6)	0.4072(6)	0.7354(3)	0.034(3)	1
O14	0.1088(6)	0.4051(5)	0.7823(3)	0.040(3)	1
D3	0.514(10)	0.889(6)	0.9136(25)	0.025	0.16(2)
D5	0.654(14)	0.75	0.4740(32)	0.025	0.16(3)
D7	0.485(8)	0.822(4)	0.5636(32)	0.025	0.18(2)

[a] T-atoms were refined as a mixture of Si and Al.

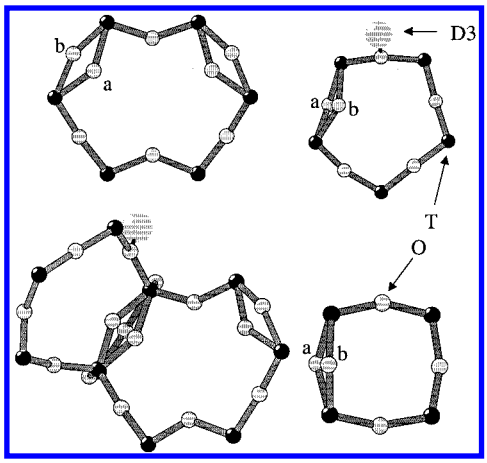

Figure 4. Alternative positions of oxygen O11. This oxygen bridges T4 and T6 and forms a common edge for a four, a five, and a six-ring. The three rings are shown separately and then all together, with the four-ring perpendicular to the plane of the figure. D3, which is attached to the five-ring is also shown.

TABLE 2: Framework Bond Lengths

T−O Bond Lengths (Å)					
1−1	1.657(5)	2−2	1.610(7)	3−6	1.583(7)
1−2	1.578(7)	2−5	1.588(4)	3−7	1.604(7)
1−3	1.615(6)	2−6	1.620(7)	3−8	1.569(5)
1−4	1.592(8)	2−7	1.585(8)	3−9	1.590(7)
4−3	1.590(7)	[a]5−8	1.591(3)	6−4	1.561(8)
4−9	1.590(7)	5−12	1.607(4)	6−13	1.598(5)
4−10	1.622(4)	[a]5−13	1.581(3)	[a]6−14	1.589(4)
4−11a	1.694(11)	5−14	1.586(5)	[a]6−11a	1.596(4)
[a]4−11b	1.586(15)			6−11b	1.661(2)

Averages for Each T-Site (Overall Average = 1.599(6) Å)					
T1−O	T2−O	T3−O	T4−O	T5−O	T6−O
1.611(7)	1.601(7)	1.587(7)	1.611(8)	1.591(4)	1.594(5)

[a] Restraint used.

occupancy by Al of the adjacent T-sites, T4 and T6, is the most likely explanation for the O11 position disorder. Several additional Fourier peaks persisted in the PXD Fourier map near O11, but attempts to refine them were unsuccessful due to the already considerable complexity of the structure. The separate O11a and O11b sites therefore appear to approximate a more complex site disorder. Disordered oxygen positions were also apparent elsewhere in the structure. A moderately sized electron-density peak (~0.2 e/Å^3) remained in the synchrotron difference Fourier map, for example, that looked like an alternate O1 site 90° out of the T−O−T plane. An attempt was made to treat this site as an alternate oxygen site, but the arrangement was unstable and tended to drift away or fall to zero occupancy. The long T−O1 bonds and the persistence of the nearby difference Fourier peak do, however, suggest the presence of site disorder and a non-negligible Al content at T1.

Just as in the case of the earlier H^+ ERS-7 structure,[34,36] the T−O distances are systematically small. On the basis of the tetrahedral Al content of the D^+ ERS-7 sample and the usual linear correlation between Al content and ⟨T−O⟩ (the average T−O distance), ⟨T−O⟩ is expected to be ~1.62 Å. However, ⟨T−O⟩ = 1.599(6) Å for the final structure reported in Tables 1 −3, and ⟨T−O⟩ = 1.594(6) Å for a completely unrestrained PXD-only refinement of the framework alone, incorrectly indicating zero Al content. A similar observation was made for the zeolite MOR.[17,48] There, the insertion of Al on either side of an oxygen bridge produces two distinct oxygen positions, the average of which naturally leads to apparently shortened T−O distances and increased T−O−T angles. Alberti et al. devised a method of calculating the Al content from framework bond lengths and angles[17] that attempts to take this disorder into account. Applying their method to the bond lengths and angles of D^+ ERS-7 yields an estimated tetrahedral Al content of 6%, which is much closer to the actual value of 7.4%. Alberti showed that Al disorder has a similar effect on the refined values of the framework parameters of many different zeolites.[14]

The final results of the combined neutron/X-ray structure refinement of D^+ ERS-7 are shown in Figures 5 and 6. Agreement indices were $R_{wp(X)}$ = 6.5%, $R_{p(X)}$ = 6.2%, $R_{B(X)}$ = 5.4%, $DW_{d(X)}$ = 0.77, $R_{wp(N)}$ = 5.6%, $R_{p(N)}$ = 4.6%, $R_{B(N)}$ = 11.6%, $DW_{d(N)}$ = 0.92, $R_{wp(C)}$ = 6.3%, $R_{p(C)}$ = 6.0%, $DW_{d(C)}$ = 0.81, and the reduced χ^2 = 1.48. The backgrounds, cell parameters, zero errors, and peak shapes were refined as was done for the Le Bail profile fits. In addition to the two scale factors, 95 structural parameters were refined including 59 positional parameters, 20 isotropic thermal parameters, one occupancy factor for the framework atoms, and eight positional parameters and three occupancy factors for the acid deuterons.

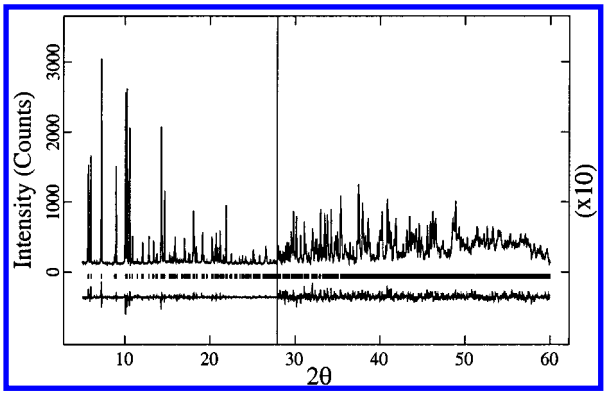

Figure 5. Observed and difference synchrotron X-ray powder diffraction patterns resulting from a combined X-ray/neutron Rietveld structure refinement of D^+ ERS-7.

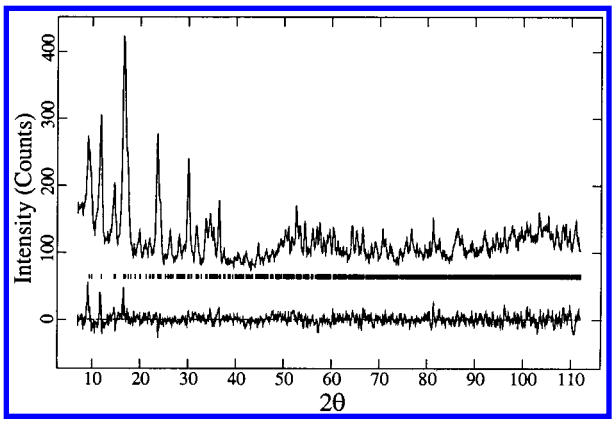

Figure 6. Observed and difference neutron powder diffraction patterns resulting from a combined X-ray/neutron Rietveld structure refinement of D^+ ERS-7.

TABLE 3: Framework Bond Angles

O−T−O Angles (Deg)					
1−1−2	111.6(5)	2−2−5	110.9(5)	6−3−7	109.3(4)
1−1−3	110.5(4)	2−2−6	108.8(4)	6−3−8	110.5(4)
1−1−4	104.4(4)	2−2−7	109.8(4)	6−3−9	108.7(4)
2−1−3	109.2(4)	5−2−6	111.0(5)	7−3−8	109.7(4)
2−1−4	112.5(5)	5−2−7	106.1(5)	7−3−9	108.3(4)
3−1−4	108.3(4)	6−2−7	110.3(4)	8−3−9	110.2(4)
3−4−9	110.2(4)	8−5−12	107.0(5)	4−6−13	108.6(4)
3−4−10	111.0(4)	8−5−13	111.1(4)	4−6−14	109.8(5)
9−4−10	112.1(5)	8−5−14	109.8(4)	13−6−14	106.4(4)
3−4−11a	119.9(5)	12−5−13	109.9(5)	4−6−11a	93.7(7)
9−4−11a	112.9(5)	12−5−14	108.1(5)	13−6−11a	116.4(5)
10−4−11a	87.5(6)	13−5−14	110.8(4)	14−6−11a	120.7(6)
3−4−11b	97.4(8)			4−6−11b	126.6(9)
9−4−11b	104.5(8)			13−6−11b	105.2(8)
10−4−11b	119.6(10)			14−6−11b	98.5(8)

Averages for each T-Site Overall Average = 109.3(5)					
O−T1−O	O−T2−O	O−T3−O	O−T4−O	O−T5−O	O−T6−O
109.4(4)	109.5(5)	109.5(4)	109.0(6)	109.5(5)	109.2(6)

T−O−T Angles (Deg) Overall Average T−O−T Angle = 152.5(6)					
1−1−1	134.1(7)	1−2−2	148.6(5)	1−3−4	151.2(5)
1−4−6	174.1(6)	2−5−2	151.4(8)	2−6−3	153.9(5)
2−7−3	152.7(5)	3−8−5	161.6(5)	3−9−4	157.6(5)
4−10−4	142.0(8)	4−11a-6	140.3(10)	4−11b-6	144.8(16)
5−12−5	156.9(7)	5−13−6	153.7(5)	5−14−6	155.1(6)

Final lattice parameters were a = 9.7843(1) Å, b = 12.3676(1) Å, and c = 22.8336(2) Å.

Brønsted Acid Site Geometries. Many ab initio quantum mechanical calculations of zeolitic Brønsted acid sites have been

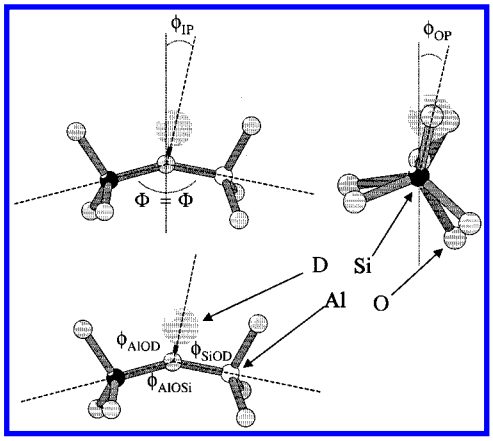

Figure 7. Illustrations of a Brønsted acid deuteron covalently bonded to a framework oxygen. The angles needed to characterize the local acid-site geometry are indicated.

TABLE 4: Acid-Site Geometries

parameter	D3(ERS-7)	D5(ERS-7)	D7(ERS-7)	calcd.
T′	T1	T2	T4	
T″	T4	T2	T6	
$r_{O-T'}$ (Å)	1.615(6)	1.588(4)	1.585(8)	1.70(2)
$r_{O-T''}$ (Å)	1.590(7)	1.588(4)	1.604(7)	1.945(2)
r_{O-D} (Å)	1.01(6)	0.91(7)	0.98(5)	0.964(4)
$\phi_{T'-O-T''}$ (°)	151.2(5)	151.4(8)	152.7(5)	131.5(5)
$\phi_{T'-O-D}$ (°)	102(6)	103.5(8)	89(5)	96.4(4)
$\phi_{T''-O-D}$ (°)	103(6)	103.5(8)	118(5)	117.5(3)
ϕ_{IP} (°)	1.7(13)	0	7.5(18)	6.0(1)
$\lvert 360° - \phi_{Sum} \rvert$ (°)	3.8(6)	1.6(8)	0.3(5)	14.6(4)
ϕ_{OP} (°)	39(18)	19(7)	34(16)	44(1)

carried out,[6−9,21−24,49−52] a number of which have indicated that the framework hydroxyl (H−O) associated with a Brønsted acid site should lean toward the Al side of the Si−O−Al angle and somewhat out of the Si−O−Al plane. The in-plane deviation from the Al−O−Si angle bisector (toward the Al side) is referred to here as ϕ_{IP}, and the deviation from the Al−O−Si plane is referred to as ϕ_{OP}. The geometry of these two angles is illustrated in Figure 7. It is straightforward to show that

$$\sin(\phi_{IP}) = 2(\cos(\phi_{AlOD}) - \cos(\phi_{SiOD}))/(1 - \cos(\phi_{AlOSi}))$$

and

$$\sin(\phi_{OP}) = \zeta^{1/2}/\sin(\phi_{AlOSi})$$

where

$$\zeta = 1 - \cos^2(\phi_{AlOSi}) - \cos^2(\phi_{AlOD}) - \cos^2(\phi_{SiOD}) + 2\cos(\phi_{AlOSi})\cos(\phi_{AlOD})\cos(\phi_{SiOD})$$

The in-plane angle, ϕ_{IP}, deviates from zero only if ϕ_{AlOD} differs from ϕ_{SiOD}, and ϕ_{OP} deviates from zero only if the sum of all three angles centered on the oxygen, $\phi_{sum} = \phi_{AlOSi} + \phi_{AlOD} + \phi_{SiOD}$, deviates from 360°.

The Brønsted acid sites of ERS-7 provide an excellent opportunity to test these first-principles calculations. The relatively low symmetry of the ERS-7 framework places two of its three acid sites (D3 and D7) on fully general positions within the unit cell, where both ϕ_{IP} and ϕ_{OP} can be measured. Sauer et al.[49−51] and Kazansky[52] compared the results of several studies and presented representative values of each of the three bond distances and three bond angles centered about the protonated oxygen. In Table 4, these "recommended" geometries are compared to those of the three acid sites of D^+ ERS-7. The two T-sites associated with each acid site were generically referred as T′ and T″. On the basis of the ab initio calculations, the smaller of the two D−O−T angles was assumed to correspond to Al at each site.

A comparison to theoretical acid-site geometries was not completed without difficulties. Because of low occupancy and disorder, the T−O bond lengths of our fractionally deuterated oxygens were approximately equal to values that were expected for a siliceous zeolite, rather than reflecting the large calculated values, Al−O = 1.94 Å and Si−O = 1.70 Å. And as discussed above, the T−O−T angles were large, rather than reflecting the ∼10° decrease that was predicted to occur upon protonation.[24] But fortunately, the acid deuteriums themselves are not averaged together with a majority background of "nonacidic" deuterium sites. So the O−D distances and T−O−D angles offer a cleaner comparison with theoretical values. Even so, these parameters are subject to averaging over Al-siting disorder in the surrounding framework. Locally, the proton may lean to one side or the other, depending on the location of the Al atom in a disordered-Al system. If the two T-sites that are linked to a given framework hydroxyl are crystallographically distinct, and if Al prefers one site over the other, then the acid site should preferentially lean toward the Al-preferred side, and thus, ϕ_{IP} should be detectable from an PND structure refinement. But when the bridging oxygen lies on a mirror plane between two identical T-atoms, as is the case for each of the framework oxygens of zeolites FAU, CHA, and RHO, the two adjacent T-sites are crystallographically identical; as a result, the Al cannot prefer one site over the other. The small displacement angles, $+\phi_{IP}$ and $-\phi_{IP}$, then have an equal probability, so that the average displacement is zero, though the thermal parameter may appear somewhat enlarged in order to accommodate the disorder.

Consider the D3 acid site first. The fact that ϕ_{IP} was nearly consistent with zero at D3 suggests that Al exists at both the T1 and T4 sites in similar proportions. Thus despite the favorable lack of mirror-plane symmetry, similar Al preferences for the two adjacent T-sites may be preventing the measurement of ϕ_{IP}, which may be significant locally. One of the acid sites observed in D^+ FER[32] is bonded to a general-position oxygen (D1), but it likewise yielded a near-zero ϕ_{IP} tilt angle. In contrast, the D7 acid site of D^+ ERS-7 demonstrates a large in-plane tilt of 7.5(18)°, which is nicely comparable to the ab initio calculated value of 6.0°. Only this D7 site offers a clear indication of Al preference for one its two adjacent T-sites (T4 over T6 in this case).

Though ϕ_{IP} is not easily determined for acid sites that are between identical T-sites, it is still possible for the out-of-plane tilt angle to systematically prefer one side of T−O−T plane. The D5 acid site of ERS-7, for example, demonstrates such a tilt, as do the acid sites in H^+ SSZ-13, D^+ RHO, and D^+ FER. The ϕ_{OP} values of the D3 and D7 sites of D^+ ERS-7 are both consistent with the ab initio calculated value of 44(1)°, while that of D5 is somewhat smaller. These ϕ_{OP} values are comparable to the out-of-plane tilts that we estimate for the D^+ RHO acid site, observed by Fischer et al.:[29] 20(8)° for their dry-calcined sample and 35(2)°for their steam-calcined sample, as well as those estimated by Smith et al.[30] for H^+ SSZ-13: 19° for D1 and 45° for D2. The variations that are observed in these angles may be the result of averaging over disordered positions associated with different Al arrangements in the surrounding framework. They may also be a result of weak hydrogen bonding to other framework oxygens, as described for SSZ-13.[30] The D−O bond lengths in Table 4 all refined to values

TABLE 5: D−O Distances to Other Neighboring Oxygens (Å)

D3	O2 2.42(10)	O9 2.50(10)	
D5	O6 2.46(1)	O6 2.46(1)	
D7	O5 2.08(7)	O7 2.78(5)	O9 2.65(8)

near the expected value of 1 Å. The D−O distances to other neighboring oxygens appear in Table 5.

The esd's in Table 4 were computed by standard statistical error-propagation methods, with the exception of ϕ_{OP}. Because standard linearized error-propagation methods break down near $\phi_{Sum} = 360°$ where the partial derivatives of ϕ_{OP} diverge, the values and esd's of ϕ_{OP} were instead simulated by statistical methods. For each acid site, 1000 sets of random-input angles were generated on the basis of the refined bond angles and esd's (assuming normal error distributions). The value of ϕ_{OP} was then calculated for each random trial set, and the mean and standard deviation of the resulting ϕ_{OP} distributions were determined. These values for ϕ_{OP} differed significantly from the directly calculated values, but they accurately reflect the rather large esd's of the measured bond angles from which they are derived.

Conclusions

The use of a simultaneous X-ray/neutron Rietveld refinement has been demonstrated in the determination of the Brønsted acid sites of a surprisingly complex new acidic zeolite, ERS-7. Lattice parameters, backgrounds, and profile parameters were first refined using the Le Bail method, the framework was refined, and acid sites were finally included in the model. Acid deuterons were located on oxygens O3, O5, and O7, with occupancies equivalent to 1.28(16), 0.64(12), and 1.44(16) deuterons per cell, respectively, for a total of 3.36(26) acid sites per unit cell, which is consistent with the chemical composition if the octahedral Al, identified by ^{27}Al NMR, is taken into account. T−O bond lengths suggest a site preference for Al at sites T4, T1, and possibly at T2, but not at the other three T-sites. Each of these preferred T-sites bonds to at least one of the observed acid-site oxygens: T4 to O3, T1 to O3, and T2 to O5 and O7. In addition to the Brønsted acid sites, a disordered oxygen site was identified in both the PND and PXD difference Fourier maps. Bridging oxygen O11 is disordered over at least two, and possibly more, distinct sites corresponding to different local arrangements of Al in neighboring T-sites. Evidence for similar disorder was also observed at other framework oxygen positions, though the refinement was already too complex to allow such a level of detail.

The characteristic parameters that describe the local geometry of an acid site can be divided into two groups, those that are averaged over both the acidic and nonacidic sites of the material, and those that are only defined and averaged over the acid sites. As acid-site specific parameters, the O−D distance and the two T−O−D angles lend themselves to direct comparison with theoretical calculations. These angles can then be reformulated as in-plane and out-of-plane hydroxyl tilts, ϕ_{IP} and ϕ_{OP}, which are predicted to deviate significantly from zero. Out-of-plane tilts were comparable to those tilts observed in previous studies. In-plane tilts, on the other hand, are difficult to observe unless there is a strong Al preference for one of the two adjacent T-sites. D7 is unique among the Brønsted acid sites that have been previously studied by PND in that it demonstrates a significant in-plane tilt angle. This tilt angle is comparable to the angle predicted by ab initio quantum mechanical calculations, and clearly indicates an Al preference for site T4 over T6.

Acknowledgment. This work has been supported, in part, by the MRSEC Program of the National Science Foundation, No. DMR96-32716. Work at the NSLS at Brookhaven National Laboratory was supported by the Div. of Materials Sciences, U.S. Department of Energy, under contract DE-AC02-98-CH10886. T.V. also expresses thanks to the Australian Nuclear Science Organization (ANSTO) for funding and access to experimental facilities during extended visits.

References and Notes

(1) (a) Corma, A. *Chem. Rev.* **1995**, *95*, 559. (b) Corma, A. *Chem. Rev.* **1997**, *97*, 2373.

(2) van Koningsveld, H.; Tuinstra, F.; van Bekkum, H.; Jansen, J. C. *Acta Crystallogr.* **1989**, *B45*, 423.

(3) (a) Asuquo, R. A.; Eder-Mirth G.; Lercher, J. A. *J. Catal.* **1995**, *155*, 376. (b) Maxwell, I.; Williams, C.; Muller F.; Krutzen, B. *Zeolite Catalysis−For the Fuels of Today and Tomorrow*, Selected Papers Series; Shell International Chemical Co. Ltd.: 1992. (c) Aboul-Gheit, A. K.; Menoufy M. F.; El-Morsi, A. K. *Appl. Catal.* **1990**, *61*, 283.

(4) Sie, S. T. *Stud. Surf. Sci. Catal.* **1994**, *85*, 587.

(5) van Santen, R. A. *Stud. Surf. Sci. Catal.* **1994**, *85*, 273.

(6) Brandle M.; Sauer, J. *J. Am. Chem. Soc.* **1998**, *120*, 1556.

(7) Sauer, J.; Sierka, M.; Haase, F. *ACS Symp. Ser.* **1999**, *721*, 358.

(8) Teunissen, E. H.; Duijneveldt, F. B.; van Santen, R. A. *J. Phys. Chem.* **1992**, *96*, 366.

(9) Teunissen, E. H.; van Santen, R. A.; Jansen A. P. J.; Duijneveldt, F. B. *J. Phys. Chem.* **1993**, *97*, 203.

(10) Smith, J. V.; Bennett, J. M. *Nature* **1968**, *219*, 1040.

(11) Megaw, H. D. *Acta Crystallogr.* **1952**, *5*, 477.

(12) Jamieson, P. B.; Dent Glasser, L. S. *Acta Crystallogr.* **1966**, *20*, 688.

(13) Olson, D. H.; Dempsey, E. *J. Catal.* **1969**, *13*, 221.

(14) Alberti, A. *Stud. Surf. Sci. Catal.* **1990**, *60*, 107.

(15) Ribbe, P. H.; Gibbs, G. V. *Am. Mineral.* **1969**, *54*, 85.

(16) Jones, J. B. *Acta Crystallogr.* **1968**, *B24*, 355.

(17) Alberti, A.; Gottardi, G. *Z. Kristallogr.* **1988**, *184*, 49.

(18) Mortier, W. J.; Pluth, J. J.; Smith, J. V. *Mater. Res. Bull.* **1975**, *10*, 1319.

(19) Alberti, A. *Zeolites* **1997**, *19*, 411.

(20) (a) Datka, J.; Gil, B.; Kubacka, A. *Zeolites* **1995**, *15*, 501. (b) Bordiga, S.; Lamberti, C.; Geobaldo, F.; Zecchina, A.; Turnes Palomino, G.; Otero Arean, C. *Langmuir*, **1995**, *11*, 527. (c) Makarova, A.; Wilson, A. E.; van Liemt, B. J.; Mesters, A. M.; de Winter, A. W.; Williams, C. *J. Catal.* **1997**, *172*, 170.

(21) Eichler, U.; Brandle, M.; Sauer, J. *J. Phys. Chem. B* **1997**, *101*, 10035.

(22) Kramer, G. J.; van Santen, R. A. *J. Am. Chem. Soc.* **1993**, *115*, 2887.

(23) Gibbs, G. V.; Meagher, E. P.; Smith, J. V.; Pluth, J. J. *ACS Symp. Ser.* **1977**, *40*, 19.

(24) Sierka, M.; Eichler, U.; Datka J.; Sauer, J. *J. Phys. Chem. B* **1998**, *102*, 6397.

(25) Jirak, Z.; Vratislav, S.; Bosacek, V. *Phys. Chem. Solids* **1980**, *41*, 1089.

(26) Czjzek, M.; Jobic, H.; Fitch, A. N.; Vogt, T. *J. Phys. Chem.* **1992**, *96*, 1535.

(27) Cheetham, A. K.; Eddy, M. M.; Thomas, J. M. *J. Chem. Soc., Chem. Commun.* **1984**, 1337.

(28) Baur, W. H.; Fischer, R. X.; Shannon, R. D.; Staley, R. H.; Vega, A. J.; Abrams, L.; Corbin D. R.; Jorgensen, J. D. *Z. Kristallogr.* **1987**, *179*, 281.

(29) Fischer, R. X.; Baur, W. H.; Shannon, R. D.; Staley, R. H.; Abrams, L.; Vega A. J.; Jorgensen, J. D. *Acta Crystallogr.* **1988**, *B44*, 321.

(30) Smith, L. J.; Davidson, A.; Cheetham, A. K. *Catal. Lett.* **1997**, *49*, 143.

(31) Smith, L.; Cheetham, A. K.; Morris, R. E.; Marchese, L.; Thomas, J. M.; Wright, P. A.; Chen, J. *Science* **1996**, *271*, 799.

(32) Martucci, A.; Alberti, A.; Cruciani, G.; Radaelli, P.; Ciambelli P.; Rapacciuolo, M. *Microporous Mesoporous Mater.* **1999**, *30*, 95.

(33) Martucci, A.; Cruciani, G.; Alberti, A.; Ritter, C.; Ciambelli, P.; Rapacciuolo, M. *Microporous Mesoporous Mater.* **2000**, *35−36*, 405.

(34) Campbell, B. J.; Bellussi, G.; Carluccio, L.; Perego, G.; Cheetham, A. K.; Cox, D. E.; Millini, R. *Chem. Commun.* **1998**, 1725.

(35) Bellussi, G.; Carluccio, L.; Millini, R. It. Patent Appl. MI94/A 002037, 1994.

(36) Millini, R.; Perego, G.; Carluccio, L.; Bellussi, G.; Cox, D. E.; Campbell, B. J.; Cheetham, A. K. In *Proc. 12th Intern. Zeolite Conf.*; Treacy, M. M. J., Higgins, J. B., Marcus, B. K., Eds.; Materials Research Society: Warrendale, PA, 1999; p 541.

(37) Freude, D.; Ernst, H.; Wolf, I. *Solid State Nucl. Magn. Reson.* **1994**, *3*, 271.
(38) Howard, C. J.; Ball, C. J.; Davis, R. L.; Elcombe, M. M. *Aust. J. Phys.* **1983**, *30*, 507.
(39) Maichle, J. K.; Ihringer, J.; Prandl, W. *J. Appl. Crystallogr.* **1988**, *21*, 22.
(40) Williams, A.; Kwei, G. H.; Von Dreele, R. B.; Larson, A. C.; Raistrick, I. D.; Bish, D. L. *Phys. Rev. B* **1988**, *37*, 7960.
(41) Yamamoto, A.; Onoda, M.; Takayama-Muromachi, E.; Izumi, F.; Ishigaki, T.; Asano, H. *Phys. Rev. B* **1990**, *42*, 4228.
(42) Crennell, S. J.; Owen, J. J.; Cheetham, A. K.; Kaduk, J. A.; Jarman, R. H. *Eur. J. Solid State Inorg. Chem.* **1991**, *28*, 397.
(43) Larson, A.; Von Dreele, R. B. *GSAS Manual*, Los Alamos Report No. LAUR-86-748, Los Alamos National Laboratory: Los Alamos, NM, 1986.
(44) Durbin, J.; Watson, G. S. *Biometrika* **1971**, *58*, 1.
(45) Finger, L. W.; Cox, D. E.; Jephcoat, A. P. *J. Appl. Crystallogr.* **1994**, *27*, 892.
(46) Stephens, P. *J. Appl. Crystallogr.* **1999**, *32*, 281.
(47) Cerius^2 Release 4.0; Molecular Simulations Inc.: San Diego, CA, 1999.
(48) Alberti, A.; Davoli, P.; Vezzalini, G. *Z. Kristallogr.* **1986**, *175*, 249.
(49) Sauer, J.; Kolmel, C. M.; Hill, J. R.; Ahlrichs, R. *Chem. Phys. Lett.* **1989**, *164*, 193.
(50) Sauer, J. *J. Mol. Catal.* **1989**, *54*, 312.
(51) Sauer, J.; Eichler, U.; Meier, U.; Schäfer, A.; von Arnim, M.; Ahlrichs, R. *Chem. Phys. Lett.* **1999**, *308*, 147.
(52) Kazansky, V. B. *Stud. Surf. Sci. Catal.* **1994**, *85*, 251, and references therein .